SUPPLEMENTARY MATERIAL 1

Concept and design of Martian far-IR ORE Spectrometer (MIRORES)

J. Ciazela[1], J. Bakala[2], M. Kowalinski[2*], S. Plocieniak[2], N. Zalewska[2], B. Pieterek[3], T. Mrozek[2], M. Ciazela[1], G. Paslawski[1], M. Steslicki[2], Z. Szaforz[2], J. Barylak[2], M. Kuzaj[4], A. Maturilli[5], J. Helbert[5], A. Muszynski[3], M. Rataj[2], S. Gburek[2], M. Jozefowicz[6], and D. Marciniak[1]

[1]Institute of Geological Sciences, Polish Academy of Sciences, Research Centre in Wrocław, Podwale 75, 50-449 Wrocław, Poland
[2]Space Research Centre, Polish Academy of Sciences, ul. Bartycka 18A, 00-716 Warsaw, Poland
[3]Institute of Geology, Adam Mickiewicz University, ul. Bogumiła Krygowskiego 12, 61-680 Poznań, Poland
[4]Wroclaw University of Science and Technology, Wybrzeże Stanisława Wyspiańskiego 27, 50-370 Wrocław, Poland
[5]Institut für Planetenforschung, Deutsches Zentrum für Luft- und Raumfahrt (DLR), Rutherfordstrasse 2, D-12489 Berlin, Germany
[6]European Space Foundation, Grodzka 42/1, 31 044 Kraków, Poland
*Correspondence: mk@cbk.pan.wroc.pl

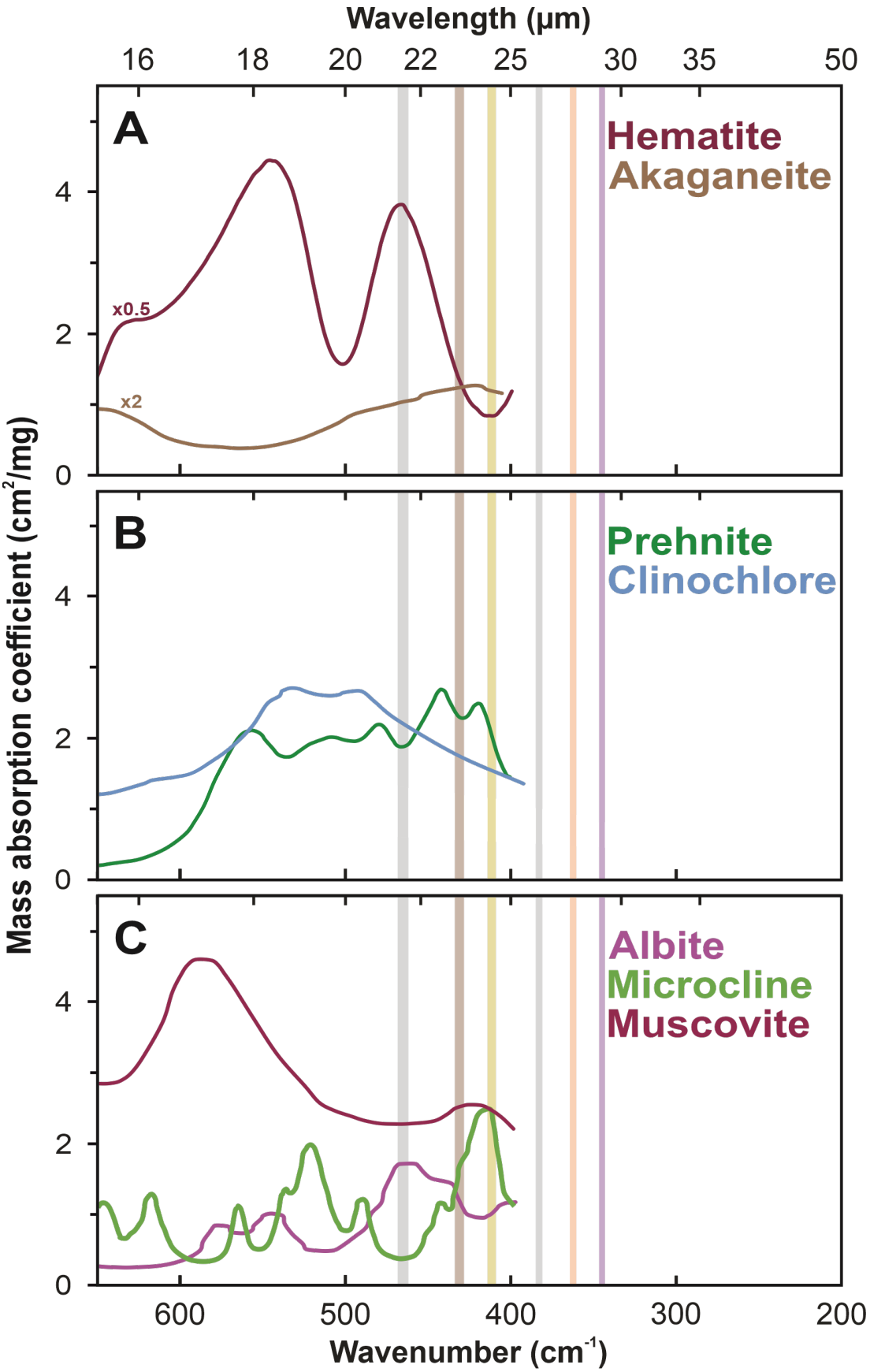
Wavelength (μm)
16
18
20
22
25
30
35
50
A
Hematite
Akaganeite
x0.5
x2
B
Prehnite
Clinochlore
C
Albite
Microcline
Muscovite
Mass absorption coefficient (cm²/mg)
0
2
4
600
500
400
300
200
Wavenumber (cm⁻¹)

Figure S1. Mass absorption coefficients of key Martian minerals with similar characteristic to sulfides classified into **(A)** oxides [1–3,4 and JHU spectral library (https://speclib.jpl.nasa.gov/documents/jhu_desc)], **(B)** secondary rock-forming minerals [3,4,5 and JHU spectral library (https://speclib.jpl.nasa.gov/documents/jhu_desc)], and **(C)** rarer primary rock-forming minerals on Mars [5]. The spectral ranges of the six detectors are marked with rectangles: orange (360–364 cm^{-1} = 27.45–27.75 µm: chalcopyrite), yellow (409–414 cm^{-1} = 24.15−24.45 µm: pyrite), brown (428–434 cm^{-1} = 23.05–23.35 µm: marcasite), gray (381–385 cm^{-1} = 25.95–26.25 µm and 462–468 cm^{-1} = 21.35–21.65 µm: reference bands), and purple (343–347 cm^{-1} = 28.85–29.15 µm: clinopyroxene).

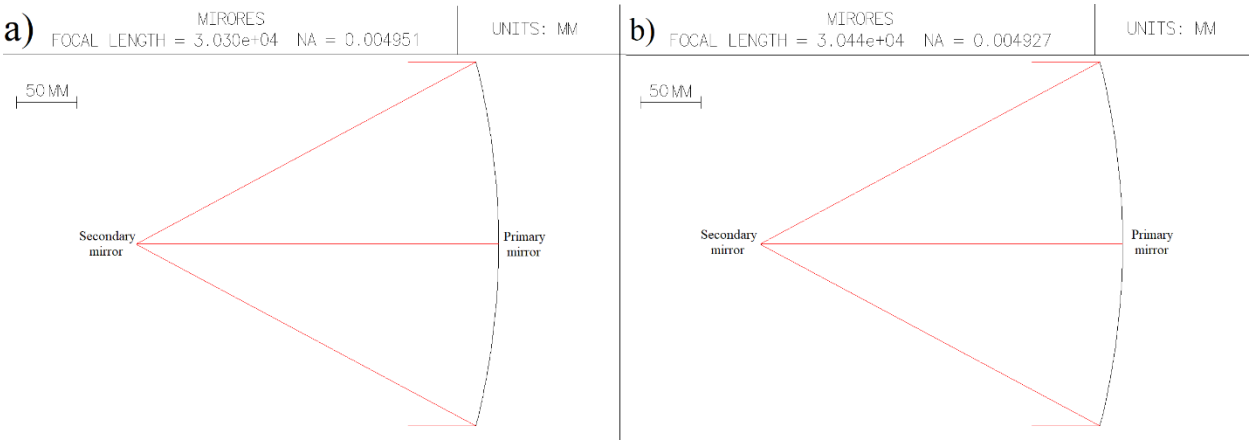

Figure S2. Ray tracing analysis corresponding to **(a)** the case with no distance shift and **(b)** to the case with a shift related the thermal expansion of both mirrors and related change in the distance between them depicted on Figure S3.D (see also the figure caption) when assumed that material will expand equally to back and front. The two images are nearly indistinguishable. The difference between the two focal lengths ($3.030 \cdot 10^4$ in **a** and $3.044 \cdot 10^4$ in **b**) is only 14 cm (0.46 rel.%). This would change the field of view by only 9 cm. NA is numerical aperture of the system and is nearly the same for **(a)** and **(b)**. The. F-number calculated as 1/(2NA) is thus 101. The analysis has been prepared in the OSLO software.

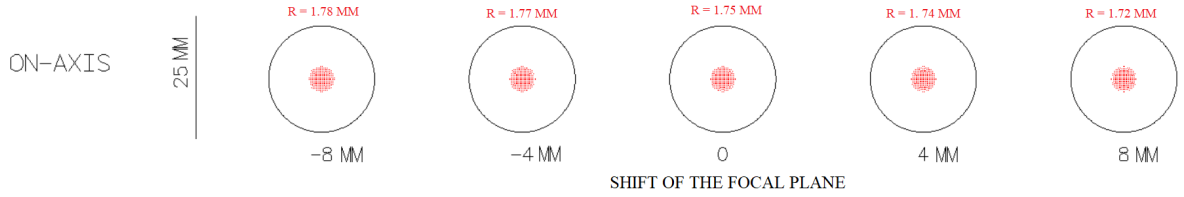

Figure S3. Optical quality of the beam in the optical axis (0, 0) when the detector is located exactly in the focal plane and when shifted by various distances. A shift from the focal by 8 mm implies the beam size is changed by 0.03 mm. The ~22 mm large black circumference represents the size of the Airy disc (corresponding to the first minimum of the Airy pattern).

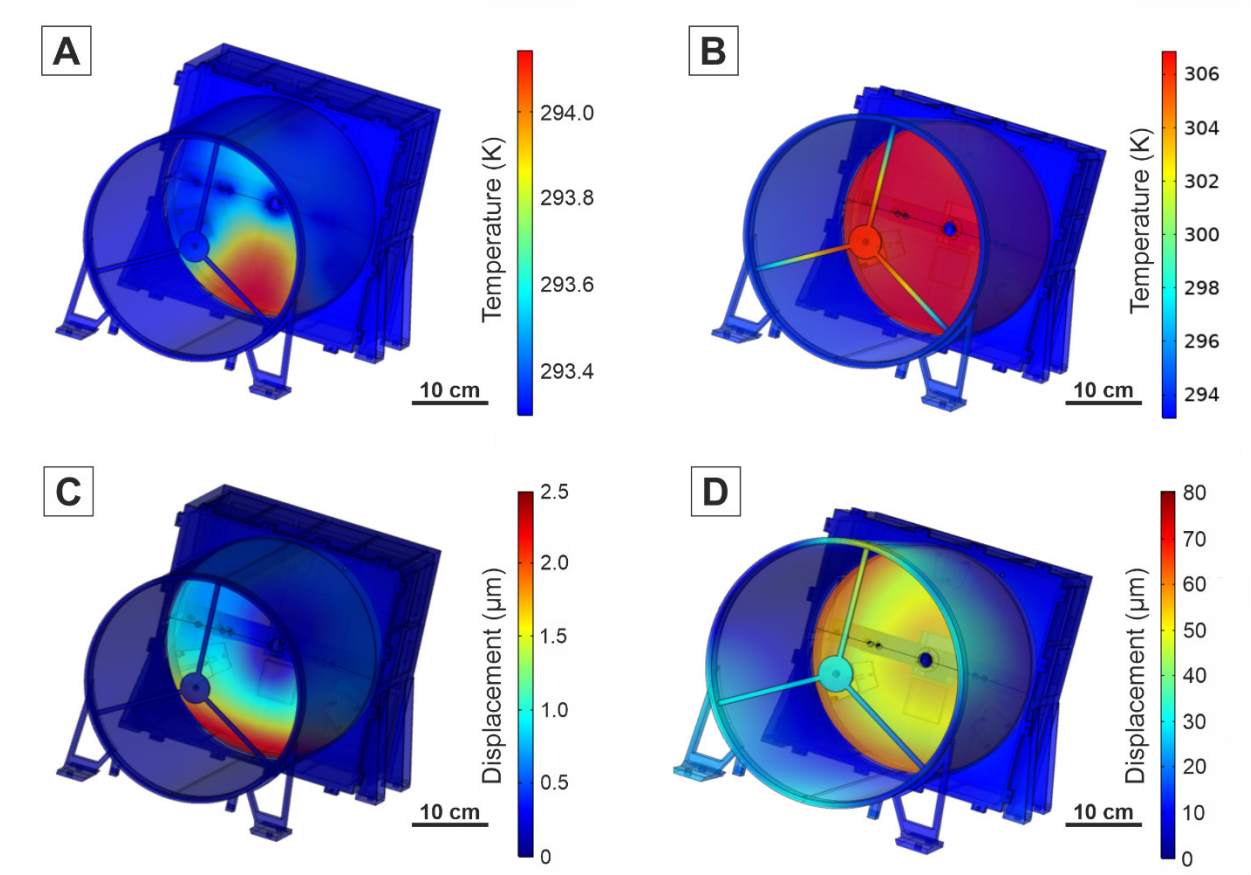

Figure S4. Thermal (A, B) and thermo-mechanical (C, D) analysis showing how changes in thermal environment induce mechanical displacement that can affect the optical performances. The assumed heat sources are 372 W/m^2 are blackbody radiation from the surface of Mars (assumed surface temperature was 293 K) and 94 W/m^2 from the reflected radiation of the Sun (assumed Mars albedo was 0.17). The instrument is assumed to operate in nadir geometry and to be shielded from direct solar radiation by the satellite shield. In simulations B and D, in which the maximum temperature reaches 307 K, it was assumed that only the electronics box has a fixed temperature of 293.15 K (20.00°C). In the remaining elements, the heat flux is dissipated by thermal conductivity. In simulations A + C, in which the temperature of the instrument is close to 293.15 K, it was assumed that the electronics box and all mechanical elements had a temperature of 293.15 K. During the construction of the device, the power flow should be adapted to how much heat could be received by the satellite but the simulations show that we should aim at achieving parameters depicted in models A + C. In the optimal scenario (A + C) thickness differences are ~1 µm, which is negligible for the optical system. However, even in the worse scenario (B + D), relative displacement between external part and internal part of the aluminium-made primary mirror (resulting in changing mirror's curvature) is ~10 µm. and the distance between primary and secondary mirror is shortened by 25 µm, which do not affect yet the focal length that is still 30 m. The focal length starts to change beyond this limit, and is estimated to be 41 m for displacements of 15 µm within the primary mirror, and 60 m for 20 µm.

a)

MIRORES
SPOT DIAGRAM

WV1-3 +△□
WV1: 24 WV2: 27 WV3: 30

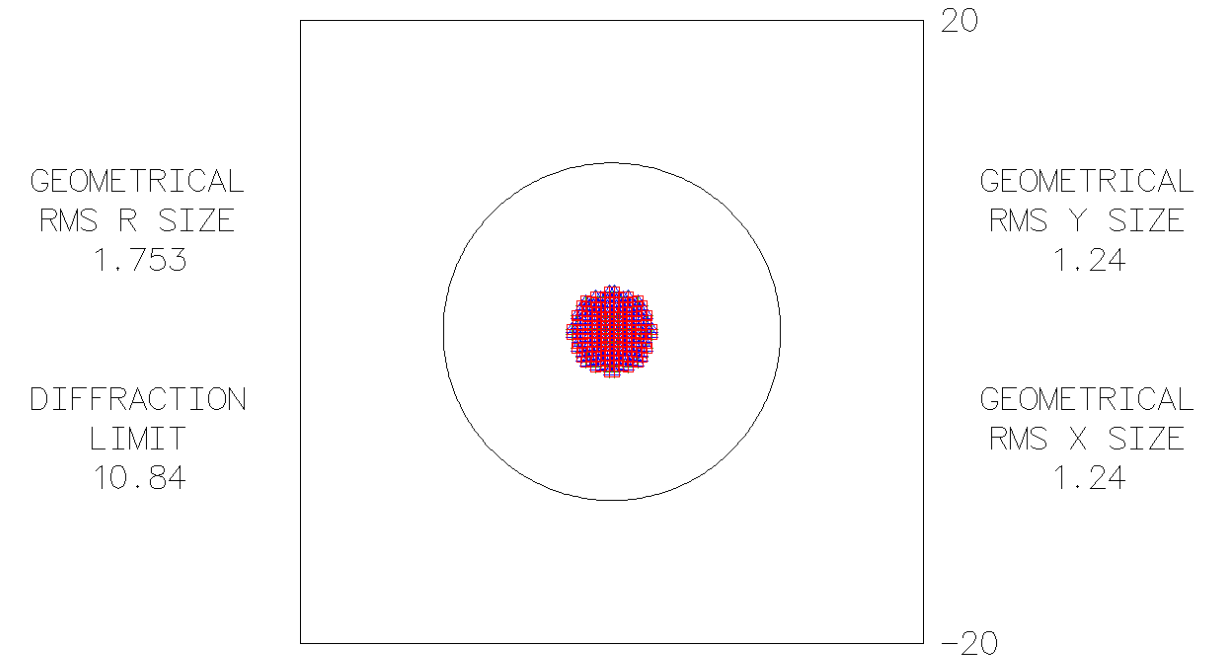

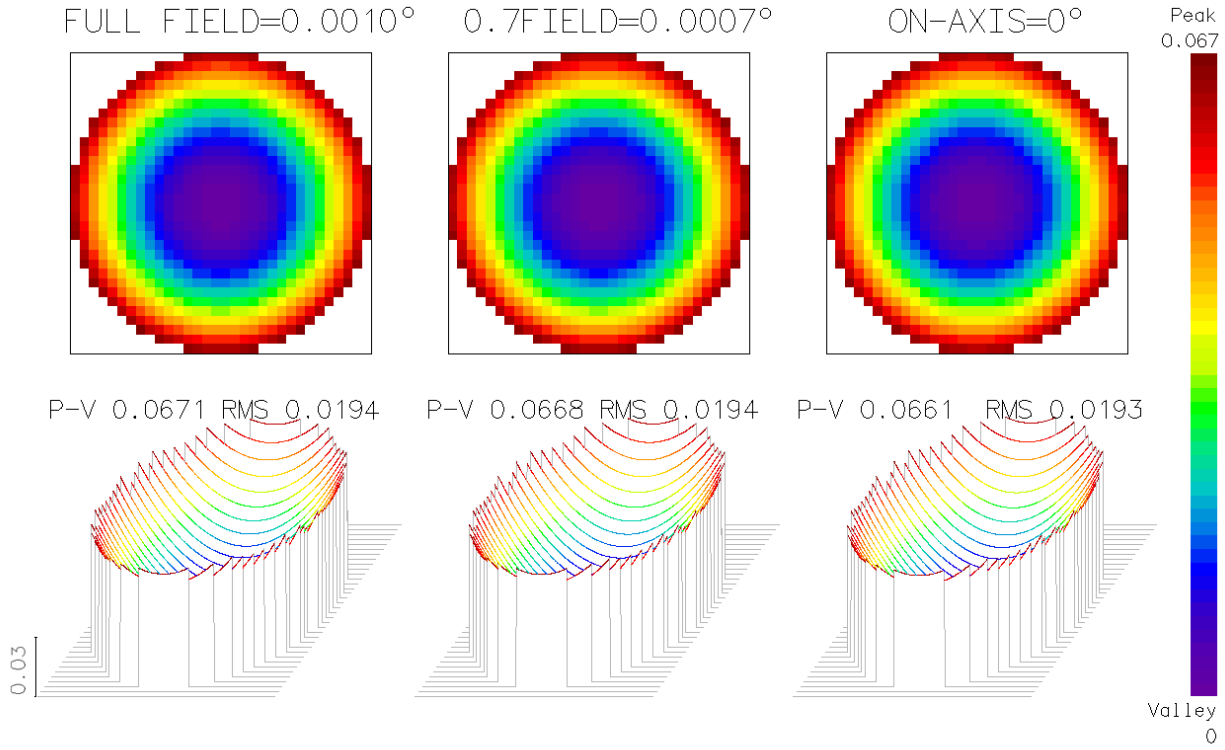

Unit: 1 = 24 µm
P-V OPD = 0.0661 waves = 1.61 µm

MIRORES
WAVEFRONT ANALYSIS

b)

MIRORES
SPOT DIAGRAM

WV1-3 +△□
WV1: 24 WV2: 27 WV3: 30

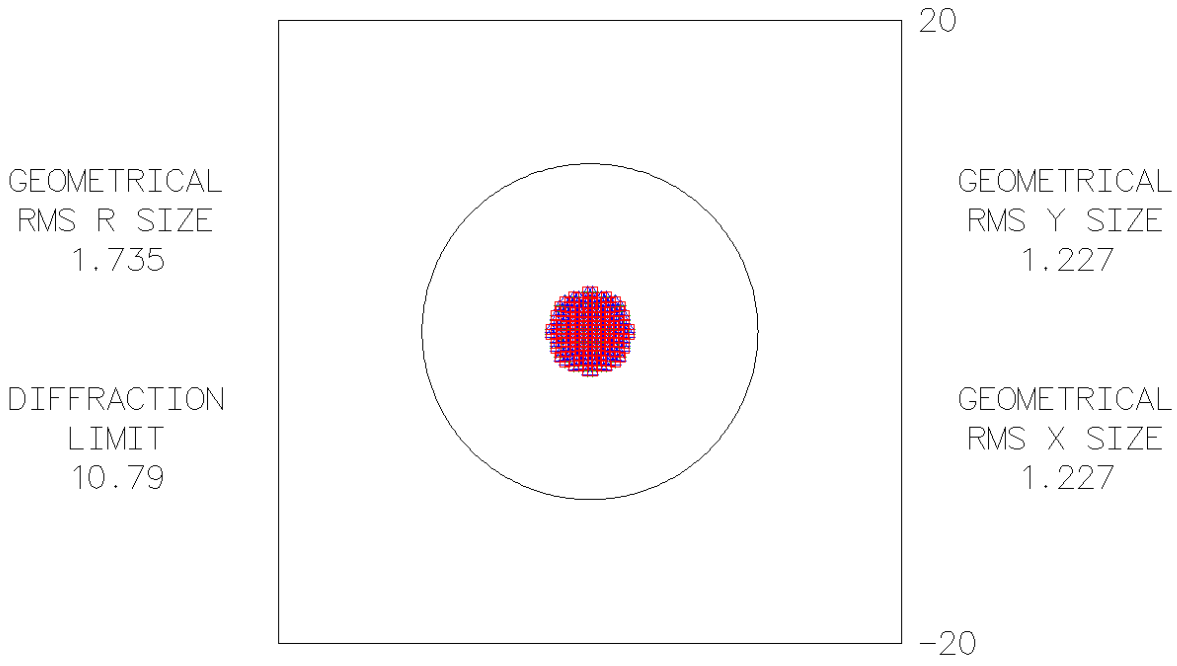

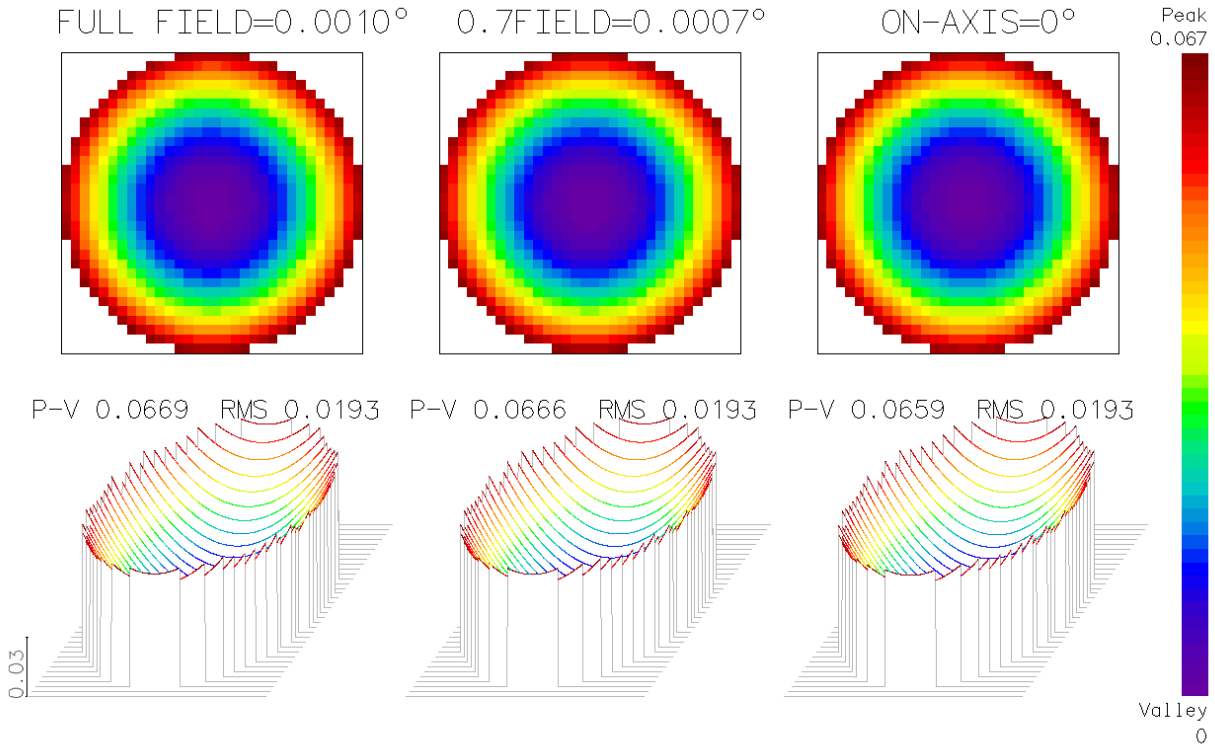

Unit: 1 = 24 µm
P-V OPD = 0.0669 waves = 1.61 µm

MIRORES
WAVEFRONT ANALYSIS

Figure S5. Tolerance analysis corresponding to **(a)** the case with no distance shift and **(b)** to the case with shift due to thermal expansion. The upper panels show the optical quality of the beam in the optical axis (0,0) (~1.7 mm in radius) as compared to the size of the Airy disc (corresponding to the first minimum of the Airy pattern) (~10.8 mm in radius). Only 0.05 mm change of diffraction limit and 0.02 mm change of spot size are visible between panels (a) and (b), which leads to a conclusion that the resolution will remain optimal during measurements. The lower panels show changes in wavefront for slight deviations (0.0010° and 0.0007°) from the optical axis. WV 1-3 are wavelengths (24 μm, 27 μm, and 30 μm) with corresponding symbols (cross, square, triangle) visible in spot diagram used for calculating spot size. RMS is random mean square, which estimates the uncertainty of computation. P-V is optical path difference (OPD) between peak (P) and valley (V) of the wavefront spot expressed in wavelength units (1 = 24 μm).

References:

1. Kendix, E.; Moscardi, G.; Mazzeo, R.; Baraldi, P.; Prati, S.; Joseph, E.; Capelli, S. Far infrared and Raman spectroscopy analysis of inorganic pigments. *J. Raman Spectrosc.* **2008**, *39*, 1104–1112, doi:10.1002/jrs.1956.
2. Murad, E.; Bishop, J.L. The infrared spectrum of synthetic akaganeite, β-FeOOH. *Am. Mineral.* **2000**, *85*, 716–721, doi:10.2138/am-2000-5-609.
3. Salisbury, J.W.; Walter, L.S.; Vergo, N. Availability of a library of infrared (2.1-25.0 μm) mineral spectra. *Am. Mineral.* **1989**, *74*, 938–939.
4. Stimson, M.; O'Donnell, M. The Infrared and Ultraviolet Absorption Spectra of Cytosine and Isocytosine in the Solid State. *J. Am. Chem. Soc.* **1952**, *74*, 1805–1808, doi:10.1143/JPSJ.28.1051.
5. Salisbury, J.W.; Walter, L.S.; Vergo, N. Mid-infrared (2.1-25 um) spectra of minerals: First edition. *USGS Open-File Rep.* **1987**, 390.
6. Brusentsova, T.; Peale, R.E.; Maukonen, D.; Figueiredo, P.; Harlow, G.E.; Ebel, D.S.; Nissinboim, A.; Sherman, K.; Lisse, C.M. Laboratory far-infrared spectroscopy of terrestrial sulphides to support analysis of cosmic dust spectra. *Mon. Not. R. Astron. Soc.* **2012**, *420*, 2569–2579, doi:10.1111/j.1365-2966.2011.20228.x.